

Predicting the J – V Curve in Organic Photovoltaics Using Impedance Spectroscopy

James I. Basham, Thomas N. Jackson, and David J. Gundlach*

Impedance spectroscopy is used as a method to predict the current–voltage curve in organic photovoltaic devices. This technique allows the quantification of the recombination rate, series resistance, carrier density, and lifetime very close to normal operating conditions. The current density is reconstructed from the generation and recombination rates. Excellent agreement with measured results is observed using this simple model. The order of recombination is found to be strongly bias dependent, displaying a shift in the dominant form of recombination from trap-mediated at low carrier densities to bimolecular at high carrier densities. Mobility is shown for a range of intensities and is found to vary significantly with fabrication conditions.

than a simple offset is needed to relate one to the other. A much better approach is to subtract the recombination rate from the generation rate, provided that recombination is also measured under one sun illumination.^[5,8] Generally speaking, it is best to make electronic measurements of solar cells at a condition as close to normal operation as possible. Carrier distribution, concentration, type, lifetime, recombination mechanism, etc. can vary widely when the same device is subjected to different bias and illumination conditions. It is not a trivial matter to ensure that a device behaves the same under measurement

conditions as when used for its intended purpose.

Several transient photovoltage techniques have demonstrated the ability to measure free carrier densities and lifetimes in solar cells and can be used to reconstruct the J – V curve.^[16–21] We demonstrate here the strengths and benefits of using impedance spectroscopy because it is quasi-steady state and can be performed at one Sun illumination. This avoids the large instantaneous fluences and potential variations required by certain transient techniques, and results in a measurement condition much closer to normal operation. The J – V curve can be predicted when the generation and recombination rates are known. In this work, we use impedance spectroscopy to quantify the recombination of a solar cell under one Sun illumination and a varied bias. This allows the J – V curve to be modeled as the generation minus recombination. We interpret carrier information from impedance spectroscopy in a way previously applied to small signal transient photovoltage measurements.^[8,16] We demonstrate that bias and illumination have a strong influence on the mechanism of recombination and charge carrier mobility. We further show the effect of processing by comparing the response of a high efficiency cell made by slow drying and annealing of a poly-3-hexylthiophene (P3HT):phenyl- C_{61} -butyric acid methyl ester (PC₆₁BM) film (referred to as “Slow AN”) to a low efficiency cell made of a fast dried, unannealed or “as cast” film (“Fast AC”). These two samples are chosen to provide a contrast between films with a highly ordered and poorly ordered microstructure, respectively. We find that changes in processing not only affect the magnitude of recombination, but also the type.

1. Introduction

Organic photovoltaics show promise as a potential low-cost, efficient and scalable technology.^[1,2] As such, there is great interest in developing predictive device models and quantitative metrics for device performance. Predicting the current density–voltage (J – V) curve is a topic of interest, as it is among the most basic device quality metrics.^[3–14] The shape of the J – V curve is heavily influenced by recombination, and it is hoped that by understanding and reducing recombination efficiencies could be further improved. A rough first approximation of the J – V curve has sometimes been to add the short circuit current to either the dark J – V curve or a diode model using parameters extracted in the dark. However, this is not the best approach as the dark condition is very different from the illuminated condition.^[15] In the dark, carriers are injected from the contacts, and may be of a single type whereas photogeneration leads to equal generation of positive and negative charges at relevant illumination conditions. The role of bimolecular recombination will change in the transition from a single carrier device to a two carrier device. The built in voltage and carrier densities and distributions also differ in the light and dark. For these reasons the curvature of the dark and illuminated J – V curves can be quite different. More

Dr. J. I. Basham, Dr. D. J. Gundlach
Semiconductor and Dimensional Metrology Division
Physical Measurement Laboratory, NIST
100 Bureau Drive
Gaithersburg, MD 20899–8120, USA
E-mail: david.gundlach@nist.gov
Dr. J. I. Basham, Prof. T. N. Jackson
Department of Electrical Engineering
Penn State University
University Park, PA 16802, USA



DOI: 10.1002/aenm.201400499

2. Background

Impedance spectroscopy is an established method for characterizing the electronic properties of dye sensitized and polymer

solar cells, for which several reviews are available.^[22–25] In this technique, a DC offset superimposed with a small AC signal across a wide frequency range are applied across the device. The response spanning many decades of frequency space reveals characteristic response times. The impedance is broken down into its real and imaginary components to discriminate between resistive and capacitive components, and fitted to a representative model circuit where the number, arrangement, and magnitude of the elements are chosen to reproduce the impedance spectrum of the device. The relationship between representative circuit element and real physical processes has been well-described in the literature. A brief review will be given here for convenience. For this work, the impedance spectra of P3HT:PC₆₁BM solar cells were measured and fitted to a model AC equivalent circuit in a fashion similar to the methods of Bisquert and coworkers,^[25–28] as shown in Figure 1a along with its DC equivalent in Figure 1b. The main difference in this work is that we use a lumped chemical capacitance where others use a distributed capacitance. Because we observe almost no frequency dispersion in the model elements of efficient devices and the time constants for recombination and transport are well-separated, both circuit models arrive at nearly identical results. A lumped capacitance, however, provides a more robust convergence during fitting and was therefore adopted because of this advantage. The circuit contains a series resistance (r_s), due to the substrate and contacts. We find that the fitted value for r_s does not vary with applied voltage and is equal to the resistance measured in an indium tin oxide (ITO)/poly(3,4-ethylenedioxythiophene):polystyrene sulfonate (PEDOT:PSS)/Ca/Al dummy stack comprised of substrate and contact materials only (approximately $3 \Omega \text{ cm}^2$). An areal capacitance and area specific resistance (C_t , r_t) represent

contact and transport effects.^[23,26,28,29] The time constant $\tau_i = C_t r_t$ is characteristic of the time to inject charge into the active layer and transport it across the device. This transport time is easily distinguished from the recombination lifetime as it is 2 to 3 orders of magnitude faster. Most importantly for modeling recombination are the chemical capacitance (C_μ) and recombination resistance (r_{rec}). The chemical capacitance is the increase in charge (Q) and carrier density (n) with a change in the quasi Fermi level (E_f), $C_\mu = q \frac{dQ}{dE_f} = q^2 L \frac{dn}{dE_f}$. It is also closely related to the filling of the density of states.^[25] Both C_μ and C_t are corrected for the geometric capacitance parallel to both, C_g , simply approximated by treating the P3HT:PC₆₁BM film as a dielectric with $C_g = \frac{\epsilon A}{L} = 25 \text{ nF cm}^{-2}$, where A is the device area and L is the active layer thickness. Because impedance spectroscopy measures the response to an AC signal, the measured capacitance corresponds to the fastest responding carrier. For this material system it is assumed that we measure the electrons in PC₆₁BM, since in neat films they have a higher mobility ($10^{-3} \text{ cm}^2 \text{ V}^{-1} \text{ S}^{-1}$)^[30] than holes in P3HT ($10^{-5} \text{ cm}^2 \text{ V}^{-1} \text{ S}^{-1}$).^[31] We are also constrained to measuring the mobile charge in the device, as fixed charges will not respond to the AC signal. Because charge is likely transported via hopping given the low mobilities involved, our definition of “mobile” includes localized charges that are able to respond at the measurement frequency, but not carriers which remain deeply trapped for longer than $\approx 1 \text{ ms}$. By integrating the chemical capacitance across the shift in the quasi Fermi energy, the increase in the concentration of the faster carrier type can be calculated as

$$n = \frac{1}{L} \int C_\mu dE_f + n_0 = \frac{1}{qL} \int C_\mu \alpha dV + n_0 \quad (1)$$

where C_μ is the chemical capacitance, E_f is the quasi Fermi level, V is the applied potential, q is the elementary charge, and α is a proportionality constant relating the voltage to the shift of the quasi Fermi level for one carrier type. n_0 is the carrier concentration at the lower bound of integration. We begin integrating at $V = 0$ (short circuit) so that n_0 can be approximated as the charge carrier flux at one Sun times the transit time, $\frac{1}{qL} J_{\text{sc}} r_t C_t$ resulting in a value of $n_0 = 10^{15} \text{ cm}^{-3}$. C_μ and n for the “Slow AN” cell are plotted in Figure 1c. The assumption is made that the contacts are ohmic, and that the applied bias is able to shift the Fermi levels directly in the bias range used, approximately 0 V to 700 mV, just above V_{oc} . While some deviation from a constant relation is expected due to non-ideal Schottky barriers, fixed charge, etc., we find that in this particular range the approximation is adequate in high efficiency cells to produce an accurate model. The open-circuit voltage is the sum of the shifts in electron and hole Fermi levels, $-q \partial V_{\text{oc}} = \partial E_{f_n} - \partial E_{f_p}$.^[27] Because we measure the applied voltage instead of measuring the quasi Fermi level directly, we scale the voltage in Equation (1) by the factor α to approximate the Fermi level shift for electrons in PC₆₁BM. For a symmetric density of states in P3HT and PC₆₁BM one would assume equal shift in each material and a value of 0.5 for α . Because the effective density of states is known to be higher in PC₆₁BM than P3HT it is reasonable to expect less shift of the Fermi level in PC₆₁BM and a value of α less than 0.5. We choose to treat α as a fitting parameter for best agreement between the recombination rate at open

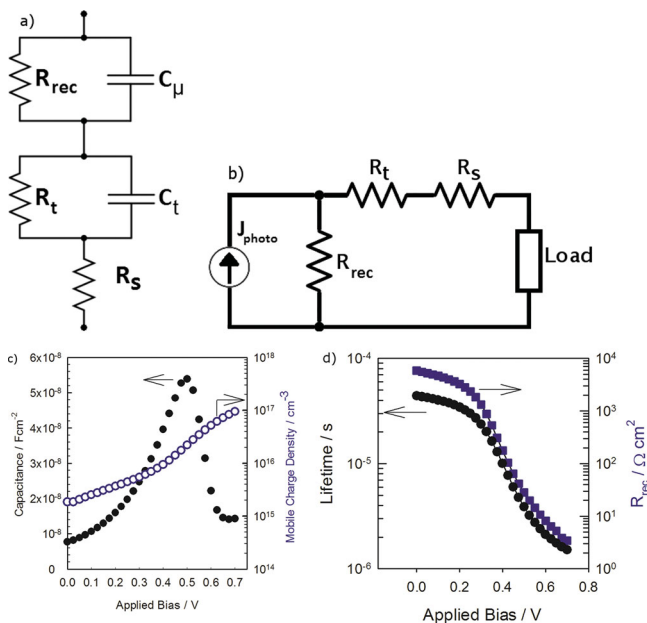


Figure 1. Equivalent circuits diagrams for a) impedance spectroscopy (AC) and b) J - V curve reconstruction (DC) 1c. Magnitude of chemical capacitance C_μ and carrier density n calculated for $\alpha = 0.3$ in the Slow AN device. 1d. The lifetime $\tau(n) = r_{\text{rec}} \times C_\mu$ (circles) and recombination resistance r_{rec} (squares) in the Slow AN device.

circuit and the generation rate at short circuit, and will later determine a more precise value.

Another important equivalent circuit element, the recombination resistance, models the rate of recombination in the cell. The current which flows through the recombination resistor in the DC equivalent circuit (Figure 1b) is the recombination current. The magnitude is a strong function of bias as a reverse bias causes carriers to be swept out before they have time to recombine, while biasing at open circuit causes all generated carriers to recombine. It is related to the cell's characteristic response time, which is also the mobile carrier lifetime τ_{by} [25,26]

$$\tau(n) = r_{\text{rec}} C_{\mu} \quad (2)$$

τ and r_{rec} for the "Slow AN" cell are plotted in Figure 1d. The lifetime is not constant and will decrease with increasing carrier density. This measure of the mobile carrier lifetime is then used to define the recombination rate (R), using the carrier density from Equation (1) and lifetime from Equation (2):

$$R = \frac{n - n_0}{\tau(n)} \quad (3)$$

where R is the volume averaged increase in recombination rate. Again, we choose n_0 to be the carrier density at short circuit because this will be a small value, and because this choice allows us to use the short circuit current to derive a net generation rate. We prefer this method of quantifying recombination over others, as it does not assume a fixed relation of the recombination rate to carrier density a priori, for example the linear dependence assumed for trap mediated recombination, or the n^2 dependence assumed for Langevin or bimolecular recombination. Simple accounting using the continuity equation gives the result that the J - V curve will be the difference between generation and recombination at each particular bias point,[5]

$$G - R = \frac{-J(V)}{qL} \quad (4)$$

where G , the generation rate is taken for simplicity to be a constant defined as $G = \frac{-J_{\text{sc}}}{qL}$. J_{sc} is determined by measuring the current under illumination and 0 V bias using a source-measure unit immediately preceding the impedance measurement. More specifically, G is a measure of the generated charge which is collected at the electrodes, actually being the bottom bound on the generation rate. For efficient cells it has been shown that the internal quantum efficiency is near unity, making this approach a close estimate of the total generation rate.[32] The initial assumption made here is that the generation rate is not field dependent. This can be valid for high quality cells with high fill factors and shunt resistances, though exploration of some systems has suggested that a field-dependent generation rate (or field-assisted extraction) could be responsible for low fill factors.[5-7,33] The modeled J - V curve will have a slightly higher fill factor because of the assumption of field-independent generation, though we observe only a small disagreement, suggesting that this is a valid assumption. Measurement of low performance cells with low shunt resistances

have shown generation will be field dependent, to be discussed later. Equation (4) includes the convention that current will be negative at short circuit, introducing a negative sign on the right hand side. Solving for $J(V)$ results in

$$J(V) = -qLG + qLR(V) \quad (5)$$

Because we can easily measure J_{sc} we substitute the approximation $G = \frac{-J_{\text{sc}}}{qL}$ into Equation (5) for the more simple expression

$$J(V) = J_{\text{sc}} + qLR(V) \quad (6)$$

The DC equivalent circuit embodied in Equation (6) is the same depicted in Figure 1b. The photogenerated charge is embodied by the current source, J_{photo} .

3. Results

In order to correctly scale the magnitude of recombination, we must select an appropriate value of α in Equation (1) to relate the total applied potential to the Fermi potential shift in PCBM only. As a starting point, we assume a symmetric density of states, meaning half of the Fermi level shift is in PCBM and $\alpha = 0.5$. This yields the blue circles shown in Figure 2, and proves to be a slight overestimate of the carrier density. To determine α , we set $J(V_{\text{oc}}) = 0$ using Equation (6) and solve for α . This gives a value of $\alpha = 0.3$. Specifically, this value matches the modeled open circuit potential to the measured value by matching the best estimate of the generation rate (from the current at open circuit) to recombination at open circuit where $G = R$. This result indicates that the Fermi level shifts more in P3HT than in PCBM, as expected from the density of states argument made earlier. The modeled J - V curve using $\alpha = 0.3$, shown in Figure 2 ("X" symbols), shows excellent agreement with that measured in the traditional fashion using a source measurement unit (solid line). The predicted fill factor and open-circuit potential match the measured values within about 2%, shown in Table 1. The quality of the fit is high, having a coefficient of determination $R^2 = 0.988$.

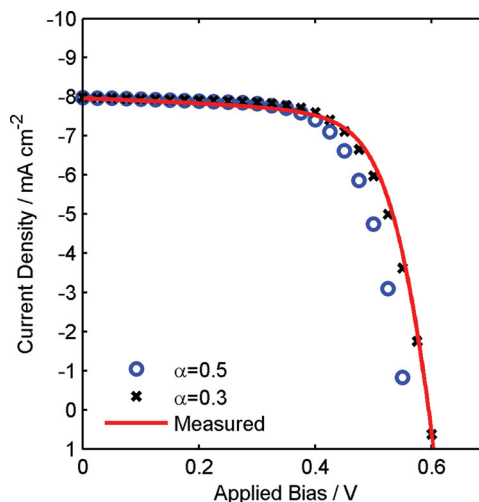


Figure 2. J - V curve reconstruction from Equation (6).

Table 1. Values extracted from a measured J - V curve vs. those predicted by the model.

	Measured Value Slow AN	Modeled Value Slow AN	Measured Value Fast AC	Modeled Value Fast AC
J_{sc} [mA cm^{-2}]	-7.95		-2.33	
V_{oc} [mV]	594	594	574	574
Fill factor [%]	69.0	67.6	44.8	44.7
Efficiency [%]	3.26	3.20	0.60	0.60

The approximation of field-independent generation works very well in the case of the high efficiency cell modeled in Figure 2. However, morphology plays an important role in charge separation and cells without ideal phase separated morphology can exhibit a strong field dependence of the generation rate. In order to demonstrate this, Fast AC devices were made in a way which caused the P3HT:PC₆₁BM film to dry quickly, resulting in a more finely mixed distribution of P3HT and PC₆₁BM. No annealing was carried out, as this would have served to cause phase separation. All other aspects, including contacts and blend ratio were the same. This film structure is closer to a single mixed phase than the bicontinuous bulk heterojunction present in the first device. Equation (6) overestimates the fill factor because geminate recombination occurs on a time scale too fast to be seen via impedance spectroscopy and is therefore not included in the measured recombination rate. In order to include geminate recombination, we effectively subtract it from the generation rate with a modified form of Equation (6):

$$J(V) = J_{sc} \left(1 - \gamma \frac{V}{L} \right) + qLR(V) \quad (7)$$

in which the newly introduced factor γ describes the strength of the field dependence of the generation rate. The quantity V/L is used to approximate the changing electric field as a uniform potential drop across the bulk. This is a convenient definition, although it should be expected that the potential will predominantly drop over a smaller region. This observed relationship could have a few different physical origins. For one the exciton dissociation rate could be linearly dependent on the electric field, causing the rate of geminate recombination to increase as open circuit is approached. We expect the phenomenon responsible for this loss is outside the timescale of the measurement (20 Hz to 2 MHz) or it would be included in the recombination term. A combination of high series and low shunt resistance can lead to a similar change in the shape of the J - V curve, however we do not observe a change in the series resistance between the Slow AN and Fast AC devices. The dark current at -1 V reverse bias is below 0.01 mA cm^{-2} for both devices, excluding the possibility of a true resistive shunt pathway. Using Equation (7) we are able to model the J - V curve of the Fast AC device with a more appropriate fill factor, seen in Figure 3. When including the factor γ our prediction is again able to match the observed values for fill factor and efficiency almost exactly with $\alpha = 0.18$ and $\gamma = 7.5 \times 10^{-4} \text{ cm V}^{-1}$. The quality of fit is high with $R^2 = 0.997$ while still maintaining the condition

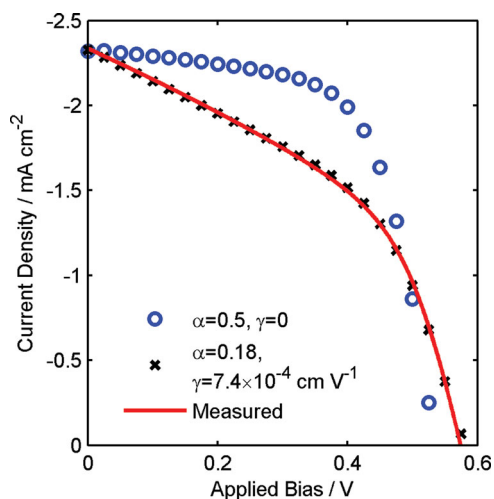


Figure 3. Modeled J - V curve for Fast AC device incorporating field-dependent generation.

that the open circuit potentials must match. The large value of γ indicates that charge extraction is heavily dependent on the electric field. At the maximum power point 61% of the current loss is due to the field dependence of charge extraction.

Returning to the Slow AN cell, we include the fitting parameter γ to explore the possibility of geminate recombination in our more efficient device. By freely varying α and γ to minimize error, we find an optimized values of $\alpha = 0.27$ and $\gamma = 4.6 \times 10^{-7} \text{ cm V}^{-1}$. For comparison, at the max power point of the Slow AN cell only about 2% of the total current loss can be ascribed to the field dependence, suggesting that it is not a determining factor in overall cell performance. It also explains why fitting with Equation (6) which lacks a term for field dependence is still able to produce a good fit.

Determining that recombination in the Slow AN cell must be predominantly non-geminate, we now seek further detail. The recombination rate, shown in Figure 4a follows a power law dependence on carrier concentration, $R \propto n^\delta$, where δ is the order of recombination.^[17,34,35] Insight into the recombination mechanism can be gained from the order of recombination. Generally, an order of 1 implies recombination via deep traps, 2 implies bimolecular recombination, and higher orders imply surface recombination or non-ideal carrier gradients with an extent approaching the active layer thickness.^[36] In Figure 4b we plot the local order of recombination using the relation^[36]

$$\delta(n) \equiv \frac{d \log(R)}{d \log(n)} \quad (8)$$

In calculating n in the dark, we use the same value of $\alpha = 0.3$ calculated under illumination and find good agreement between the measured and predicted dark J - V curves (not shown). It is interesting to see that there are stark differences between the order of recombination and therefore mechanism of recombination not only between the same cell in the dark and under illumination, but also close to short circuit and close to open circuit. Under illumination, we see that although generation is the same at all points the order of recombination is close to one at short circuit. Carriers are swept out of

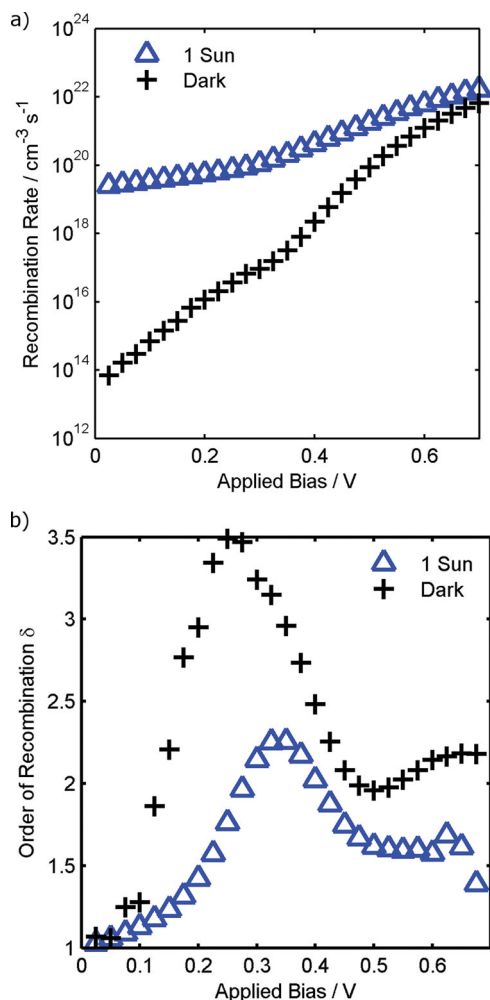


Figure 4. Differences in the Slow AN device in a) recombination rate as a function of applied bias and b) order of recombination as a function of applied bias in the dark and under illumination.

the device quickly and their concentration is low, comparable to the concentration of traps, and trap-mediated recombination is the dominant process. Close to open circuit less current is extracted, raising carrier concentration to the point where carrier density is large compared to the trap state density and bimolecular recombination becomes dominant. Near V_{oc} a value of $\delta = 1.6$ is observed, indicating that both bimolecular and trap-mediated recombination are present under this condition. Applying bias will also modulate the width of the depleted region which affects the apparent order of recombination when measured via Equation (7).^[37] Because we use a spatially averaged carrier concentration this effect is not corrected, and can explain the high value of δ seen at about 0.3 V. Device models incorporating spatial inhomogeneity in carrier density show that this effect, especially in cells having a thin active layer, can result in values of δ well over 2.^[36] Additionally, a mobility which strongly increases with carrier concentration could yield values of δ above 2 when considering that Langevin recombination carries a mobility dependence, $R = \frac{q}{2} \mu_n (n) np$. To fully confirm this possibility would require knowledge of both hole and electron mobilities and concentrations in both phases

of the bulk heterojunction, however, as previous Langevin models have shown an effective medium approximation to be invalid. At open circuit where the carrier profiles are nearly homogeneous we measure an order of recombination of $\delta = 1.8$, indicating predominantly bimolecular recombination with some trap mediated recombination, in good agreement with observations of the intensity dependence of the open circuit voltage and charge extraction measurements.^[17,38]

To probe further into differences at varying illumination levels, mobility (μ) was measured as a function of illumination intensity (ϕ). We use a transit time based analysis utilizing the time constant extracted from the part of the equivalent circuit related to transport, $\tau_t = \tau_i \times C_i$:

$$\mu(\Phi) = \frac{L^2}{V_{oc}(\Phi) \tau_t(\Phi)} \quad (9)$$

Here the transit time is measured at short circuit, and V_{oc} represents the open circuit potential at the same illumination level. This would provide an upper limit to the mobility, as the width of the depleted region of the device will be somewhat less than the total device thickness. Mobility is plotted in **Figure 5** for both the high and low efficiency cell. In the high efficiency cell, mobility is initially low but quickly plateaus to a value of $3 \times 10^{-4} \text{ cm}^2 \text{ V}^{-1} \text{ s}^{-1}$ indicating that there are likely localized, with transport occurring via hopping. In the lower efficiency cells, however, mobility remains low and slowly increases with intensity. This may indicate trapping through states with a broader distribution of activation energies than the more efficient cell. Because the built in field also increases with illumination intensity, we must also consider field-induced barrier lowering for hopping. Because both films are spun from the same solution we can conclude that the differences in mobility are morphological in nature. It is likely that the high efficiency Slow AN cell has larger and more well-ordered domains that provide good percolation pathways to the collecting electrode, while the lower mobility cell will have much greater disorder and small, poorly connected domains.^[39,40] If the probability of exciton dissociation is dependent upon mobility, as many interpretations predict, then the generally low mobilities observed

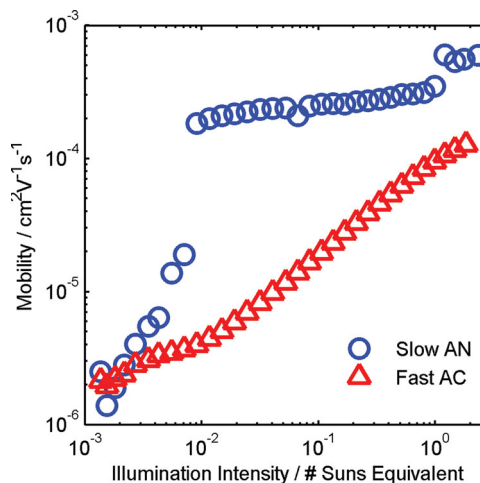


Figure 5. Mobility estimated from Equation (9).

in the low efficiency cell could explain the observation of field-dependent generation.

4. Conclusion

In conclusion this work has demonstrated a method for predicting the J - V curve using impedance spectroscopy. The recombination rate is quantified from the characteristic capacitance and resistance of the device. The shape of the J - V curve is reproduced with great accuracy because the impedance measurement is performed at nearly identical conditions to the traditional method. To emphasize the importance of this aspect the recombination rate in both the dark and under illumination is shown in Figure 4a. The discrepancy between the two can be as high as a factor of 100 due to the differences in carrier distribution, concentration, type, lifetime, and recombination mechanism mentioned previously. It is important that the method for measuring recombination incorporates the proper bias and illumination conditions, as we have shown that both have a strong effect on the recombination rate and mechanism. Therefore, impedance spectroscopy and the methods outlined in this work are particularly well suited for measuring recombination in a way consistent with Equation (6). The variation we observe with bias and intensity can explain why different methods of measuring recombination arrive at different conclusions: because the devices are not under equivalent testing conditions.^[17,41–43]

The J - V curve of a high performance cell is modeled with high accuracy while it is noted that poor performing cells are more difficult to model, requiring the inclusion of field-dependent generation. The observations are in excellent agreement with studies using transient photovoltage. The mechanism of recombination is seen to shift from trap-mediated at short circuit to mostly bimolecular near open circuit. We also observed that mobility is lower in fast dried films and slowly increases with intensity. Finally, we show that fast dried films suffer from a very strong field dependence of charge extraction, likely due to geminate recombination, and that proper film processing is key to minimizing recombination losses.

5. Experimental Section

Fabrication: Patterned ITO substrates (Thin Film Devices)^[44] were prepared by ultrasonically in acetone, isopropanol and deionized (DI) water and then dried in an oven. Clean substrates were subjected to UV-ozone treatment for 20 min. PEDOT:PSS (P VP Al 4083, Clevios) was dispensed through a 0.2 μm polypropylene filter and spin coated at 167π rad s^{-1} (5000 rpm). All further fabrication and testing was performed in an argon-filled glovebox. PEDOT:PSS films were annealed at 140 °C for 10 min. P3HT (Plexcore OS 2100, Plextronics) and PC₆₁BM (Nano-C) were dissolved overnight in 1,2 ortho-dichlorobenzene (99.8%, Aldrich) and mixed in a 5:4 w/w P3HT:PC₆₁BM solution having total dissolved solids of 15 mg mL^{-1} (Slow AN) or 30 mg mL^{-1} (Fast AC). Solutions were dispensed through a 0.45 μm PTFE syringe filter and spin coated on the prepared substrates at Slow AN films were spun at 20π rad s^{-1} (600 rpm) for 45 s (5 second ramp up) and then quickly removed and covered with a petri dish while still wet to dry over several minutes. Dry films were then annealed at 140 °C for 10 min. Fast AC films were spun at 40π rad s^{-1} (1200 rpm) for 60 s

and were not annealed. Calcium (20 nm) and aluminum (60 nm) were thermally evaporated at a rate of 2 \AA s^{-1} from a base pressure of 1.3×10^{-4} Pa (10^{-7} Torr) through a shadow mask. The active area, as defined by overlap of isolated ITO and metal contacts, was 4 mm^2 .

Characterization: Current–voltage characteristics were measured using a Keithley 2636A source meter. Illumination was provided by a Newport Oriel xenon arc lamp using AM1.5G filters. An intensity of 100 mW cm^{-2} was set with a calibrated KG filtered silicon diode. The spectral mismatch factor was measured to be 0.99.^[45] Impedance spectra were measured in the range of 20 Hz to 2 MHz using an Agilent E4980A LCR meter. A DC bias applied across the anode and cathode was superimposed with a 25 mV AC signal. During the measurement the device was illuminated by a neutral white light-emitting diode (LED; LED Engin). The intensity was set to give the same short circuit current as 1 Sun AM 1.5G illumination for “1 Sun equivalent” conditions. The spectral mismatch was calculated against a KG-filtered diode to be 1.03, for which the intensity was corrected. Impedance spectra were fitted to the circuit model by freely varying all elements except for the geometric capacitance, which was fixed at a constant 25 nF cm^{-2} for a 100 nm thick layer with a relative dielectric constant of 3. This agrees with the measured value of the fully depleted capacitance under -1 V bias in the dark.

Acknowledgements

The authors would like to thank Jason Campbell, Carsten Deibel, Behrang Hamadani, and Lee Richter for helpful discussions.

Received: March 21, 2014

Revised: April 19, 2014

Published online:

- [1] F. C. Krebs, N. Espinosa, M. Hösel, R. R. Søndergaard, M. Jørgensen, *Adv. Mater.* **2014**, *26*, 29.
- [2] J. You, L. Dou, K. Yoshimura, T. Kato, K. Ohya, T. Moriarty, K. Emery, C.-C. Chen, J. Gao, G. Li, Y. Yang, *Nat. Commun.* **2013**, *4*, 1446.
- [3] A. Wagenpfahl, D. Rauh, M. Binder, C. Deibel, V. Dyakonov, *Phys. Rev. B* **2010**, *82*, 115306.
- [4] C. G. Shuttle, R. Hamilton, B. C. O'Regan, J. Nelson, J. R. Durrant, *Proc. Natl. Acad. Sci. USA* **2010**, *107*, 16448.
- [5] G. F. A. Dibb, T. Kirchartz, D. Credgington, J. R. Durrant, J. Nelson, *J. Phys. Chem. Lett.* **2011**, *2*, 2407.
- [6] B. M. Savoie, B. Movaghar, T. J. Marks, M. A. Ratner, *J. Phys. Chem. Lett.* **2013**, *4*, 704.
- [7] G. F. A. Dibb, F. C. Jamieson, A. Maurano, J. Nelson, J. R. Durrant, *J. Phys. Chem. Lett.* **2013**, *4*, 803.
- [8] P. P. Boix, A. Guerrero, L. F. Marchesi, G. Garcia-Belmonte, J. Bisquert, *Adv. Energy Mater.* **2011**, *1*, 1073.
- [9] T. Kirchartz, B. E. Pieters, J. Kirkpatrick, U. Rau, J. Nelson, *Phys. Rev. B* **2011**, *83*, 115209.
- [10] M. Soldera, K. Taretto, T. Kirchartz, *Phys. Status Solidi A* **2012**, *209*, 207.
- [11] R. C. I. MacKenzie, C. G. Shuttle, M. L. Chabiny, J. Nelson, *Adv. Energy Mater.* **2012**, *2*, 662.
- [12] M. Gluecker, A. Foertig, V. Dyakonov, C. Deibel, *Phys. Status Solidi RRL* **2012**, *6*, 337.
- [13] S. R. Raga, F. Fabregat-Santiago, *Phys. Chem. Chem. Phys.* **2013**, *15*, 2328.
- [14] F. Fabregat-Santiago, J. Bisquert, E. Palomares, L. Otero, D. Kuang, S. M. Zakeeruddin, M. Gratzel, *J. Phys. Chem. C* **2007**, *111*, 6550.
- [15] T. Kirchartz, F. Deledalle, P. S. Tuladhar, J. R. Durrant, J. Nelson, *J. Phys. Chem. Lett.* **2013**, *4*, 2371.

- [16] C. Shuttle, B. O'Regan, A. Ballantyne, J. Nelson, D. Bradley, J. Durrant, *Phys. Rev. B* **2008**, *78*, 113201.
- [17] C. Deibel, D. Rauh, A. Foertig, *Appl. Phys. Lett.* **2013**, *103*, 043307.
- [18] A. Maurano, R. Hamilton, C. G. Shuttle, A. M. Ballantyne, J. Nelson, B. O'Regan, W. Zhang, I. McCulloch, H. Azimi, M. Morana, C. J. Brabec, J. R. Durrant, *Adv. Mater.* **2010**, *22*, 4987.
- [19] A. Foertig, J. Rauh, V. Dyakonov, C. Deibel, *Phys. Rev. B* **2012**, *86*, 115302.
- [20] A. Baumann, J. Lorrmann, D. Rauh, C. Deibel, V. Dyakonov, *Adv. Mater.* **2012**, *24*, 4381.
- [21] S. A. Hawks, F. Deledalle, J. Yao, D. G. Rebois, G. Li, J. Nelson, Y. Yang, T. Kirchartz, J. R. Durrant, *Adv. Energy Mater.* **2013**, *3*, 1201.
- [22] T. Ripolles-Sanchis, A. Guerrero, J. Bisquert, G. Garcia-Belmonte, *J. Phys. Chem. C* **2012**, *116*, 16925.
- [23] J. Bisquert, F. Fabregat-Santiago, I. Mora-Seró, G. Garcia-Belmonte, S. Giménez, *J. Phys. Chem. C* **2009**, *113*, 17278.
- [24] J. Bisquert, G. Garcia-Belmonte, *J. Phys. Chem. Lett.* **2011**, *2*, 1950.
- [25] J. Bisquert, F. Fabregat-Santiago, I. Mora-Seró, G. Garcia-Belmonte, E. M. Barea, E. Palomares, *Inorganica Chim. Acta* **2008**, *361*, 684.
- [26] G. Garcia-Belmonte, A. Munar, E. M. Barea, J. Bisquert, I. Ugarte, R. Pacios, *Org. Electron.* **2008**, *9*, 847.
- [27] G. Garcia-Belmonte, P. P. Boix, J. Bisquert, M. Sessolo, H. J. Bolink, *Sol. Energy Mater. Sol. Cells* **2010**, *94*, 366.
- [28] F. Fabregat-Santiago, G. Garcia-Belmonte, I. Mora-Seró, J. Bisquert, *Phys. Chem. Chem. Phys.* **2011**, *13*, 9083.
- [29] F. Fabregat-Santiago, J. Bisquert, L. Cevey, P. Chen, M. Wang, S. M. Zakeeruddin, M. Gratzel, *J. Am. Chem. Soc.* **2009**, *131*, 558.
- [30] V. D. Mihailetschi, J. K. J. van Duren, P. W. M. Blom, J. C. Hummelen, R. A. J. Janssen, J. M. Kroon, M. T. Rispens, W. J. H. Verhees, M. M. Wienk, *Adv. Funct. Mater.* **2003**, *13*, 43.
- [31] M. Giulianini, E. R. Waclawik, J. M. Bell, N. Motta, *J. Appl. Phys.* **2010**, *108*, 014512.
- [32] S. H. Park, A. Roy, S. Beaupré, S. Cho, N. Coates, J. S. Moon, D. Moses, M. Leclerc, K. Lee, A. J. Heeger, *Nat. Photonics* **2009**, *3*, 297.
- [33] A. Foertig, J. Knierpert, M. Gluecker, T. Brenner, V. Dyakonov, D. Neher, C. Deibel, *Adv. Funct. Mater.* **2014**, *24*, 1306.
- [34] I. Montanari, A. F. Nogueira, J. Nelson, J. R. Durrant, C. Winder, M. A. Loi, N. S. Sariciftci, C. Brabec, *Appl. Phys. Lett.* **2002**, *81*, 3001.
- [35] T. Offermans, S. C. J. Meskers, R. a. J. Janssen, *J. Chem. Phys.* **2003**, *119*, 10924.
- [36] T. Kirchartz, J. Nelson, *Phys. Rev. B* **2012**, *86*, 165201.
- [37] L. Koster, E. Smits, V. Mihailetschi, P. Blom, *Phys. Rev. B* **2005**, *72*, 085205.
- [38] G.-J. A. H. Wetzelaer, M. Kuik, P. W. M. Blom, *Adv. Energy Mater.* **2012**, *2*, 1232.
- [39] B. A. Collins, J. R. Tumbleston, H. Ade, *J. Phys. Chem. Lett.* **2011**, *2*, 3135.
- [40] M. Campoy-Quiles, T. Ferenczi, T. Agostinelli, P. G. Etchegoin, Y. Kim, T. D. Anthopoulos, P. N. Stavrinou, D. D. C. Bradley, J. Nelson, *Nat. Mater.* **2008**, *7*, 158.
- [41] R. A. Street, *Phys. Rev. B* **2011**, *84*, 075208.
- [42] C. Deibel, A. Wagenpfahl, *Phys. Rev. B* **2010**, *82*, 207301.
- [43] R. A. Street, *Phys. Rev. B* **2010**, *82*, 207302.
- [44] Commercial materials, instruments, and equipment are identified in this paper to specify the experimental procedure as completely as possible. In no case does such identification imply a recommendation or endorsement by the National Institute of Standards.
- [45] V. Shrotriya, G. Li, Y. Yao, T. Moriarty, K. Emery, Y. Yang, *Adv. Funct. Mater.* **2006**, *16*, 2016.